Spin Crossover Behavior in a Series of Iron(III) Alkoxide Complexes

ARTICLE *in* INORGANIC CHEMISTRY · MARCH 2015

Impact Factor: 4.76 · DOI: 10.1021/ic503081x · Source: PubMed

8 AUTHORS, INCLUDING:

Marcos Flores-Alamo
Universidad Nacional Autónoma de México
153 PUBLICATIONS **409** CITATIONS
SEE PROFILE

Rafael Moreno-Esparza
Universidad Nacional Autónoma de México
71 PUBLICATIONS **757** CITATIONS
SEE PROFILE

Víctor Manuel Ugalde-Saldívar
Universidad Nacional Autónoma de México
40 PUBLICATIONS **350** CITATIONS
SEE PROFILE

Inorganic Chemistry

Article

pubs.acs.org/IC

Spin Crossover Behavior in a Series of Iron(III) Alkoxide Complexes

Norma Ortega-Villar,[†] Areli Yesareth Guerrero-Estrada,[†] Lucía Piñeiro-López,[‡] M. Carmen Muñoz,[§] Marcos Flores-Álamo,[†] Rafael Moreno-Esparza,[†] José A. Real,*[,‡] and Víctor M. Ugalde-Saldívar*[,†]

[†]Facultad de Química, Universidad Nacional Autónoma de México, Edificio B, Av. Universidad 3000, Coyoacán, 04510 México, D.F., México

[‡]Institut de Ciencia Molecular (ICMol), Universitat de València, C/Catedrático José Beltrán Martinez no. 2, 46980 Paterna, Valencia, Spain

[§]Departament de Física Aplicada, Universitat Politècnica de València, Camino de Vera s/n, E-46022 València, Spain

Supporting Information

ABSTRACT: The synthesis, crystal structures, magnetic behavior, and electron paramagnetic resonance studies of five new Fe^{III} spin crossover (SCO) complexes are reported. The $[Fe^{III}N_5O]$ coordination core is constituted of the pentadentate ligand bztpen (N_5) and a series of alkoxide anions (ethoxide, propoxide, *n*-butoxide, isobutoxide, and ethylene glycoxide). The methoxide derivative previously reported by us is also reinvestigated. The six complexes crystallize in the orthorhombic *Pbca* space group and show similar molecular structures and crystal packing. The coordination octahedron is strongly distorted in both the high- and low-temperature structures. The structural changes upon spin conversion are consistent with those previously observed for $[Fe^{III}N_4O_2]$ SCO complexes of the Schiff base type, except for the Fe−O(alkoxide) bond distance, which shortens significantly in the high-spin state. Application of the Slichter−Drickamer thermodynamic model to the experimental SCO curves afforded reasonably good simulations with typical enthalpy and entropy variations ranging in the intervals ΔH = 6−13 kJ mol^{-1} and ΔS = 40−50 J mol^{-1} K^{-1}, respectively. The estimated values of the cooperativity parameter Γ, found in the interval 0−2.2 kJ mol^{-1}, were consistent with the nature of the SCO. Electron paramagnetic resonance spectroscopy confirmed the transformation between the high-spin and low-spin states, characterized by signals at $g \approx 4.47$ and 2.10, respectively. Electrochemical analysis demonstrated the instability of the Fe(II) alkoxide derivatives in solution.

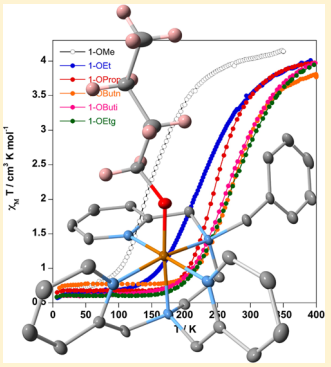

INTRODUCTION

The spin crossover (SCO) phenomenon takes place when the energy gap between the high-spin (HS) and low-spin (LS) states of pseudo-octahedral first-row transition metal complexes with electronic configurations $3d^n$ ($4 \le n \le 7$) is on the order of magnitude of the thermal energy k_BT. Thus, the metal complex can switch between the two states in a reversible, detectable, and controllable way by the action of external stimuli such as temperature, pressure, light, intense magnetic fields, or even an analyte.[1]

The SCO phenomenon was discovered by Cambi and Szegö in 1931 in a series of tris(*N*,*N*-disubstituted-dithiocarbamato)-iron(III) complexes.[2] Since then, a variety of iron(III) complexes undergoing SCO between the HS ($S = {}^5/_2$) and LS ($S = {}^1/_2$) states have been reported. Multidentate Schiff base-type ligands have proved to be the most versatile source of iron(III) SCO complexes.[1l,3] In addition, the search for diverse efficient biomimetic models derived from catechol dioxygenases,[4] cytochrome P450 oxidase,[5] lipoxygenases,[6] and related mononuclear non-heme ion enzymes[7] has afforded an "indirect" source of iron(III) SCO complexes. In this regard, $[Fe^{II,III}(R\text{-tpen})(X)]^{n+}$ type complexes, where R-tpen is the pentadentate N_5 ligand *N*-R-*N*,*N*′,*N*′-tris(2-methylpyridyl)-ethylenediamine and X is an exogenous monotopic ligand (anionic or neutral), have been the subject of intense research.[8,9] In particular, we have investigated the stability of the $[Fe^{II}(bztpen)(X)]^{n+}$ complexes against their redox properties, where bztpen is *N*-benzyl-*N*,*N*′,*N*′-tris(2-pyridylmethyl)-ethylenediamine (Chart 1). The stabilization of the ferrous state follows fairly well the expected spectrochemical series, with the least and most stable complexes having X = I^- and CN^-, respectively. This result is consistent with the solid-state structural and magnetic data obtained for the $[Fe^{II}(bztpen)(X)](PF_6)_n$ series. Halide and pseudohalide complexes (X =

Chart 1. Structure of the Ligand *N*-Benzyl-*N*,*N*′,*N*′-tris(2-pyridylmethyl)ethylenediamine (bztpen)

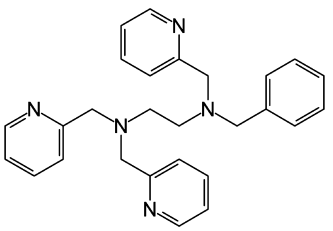

Received: December 24, 2014

DOI: 10.1021/ic503081x
Inorg. Chem. XXXX, XXX, XXX−XXX

Cl^-, Br^-, I^-, OCN^-, and SCN^-) are HS ($S = 2$), while the LS state ($S = 0$) is the stable state for X = $[N(CN)_2]^-$, CH_3CN, and CN^-. Apparently, the crossing point between the HS and LS states should be placed somewhere between SCN^- and CH_3CN or $[N(CN)_2]^-$.[10] Indeed, two-step and normal SCO behavior was observed in the solid state and in solution, respectively, for the dinuclear species $\{[Fe^{II}(bztpen)]_2[\mu\text{-}N(CN)_2]\}(PF_6)_3$.[11]

As a consequence of this systematic study, we realized that $[Fe^{II}(bztpen)(CH_3OH)](PF_6)_2$ in neutral and slightly basic methanolic solutions oxidizes under anaerobic conditions to give $[Fe^{III}(bztpen)(CH_3O)](PF_6)_2$ (**1-OMe**), which represents the first example of a methoxide Fe^{III} complex exhibiting SCO in the solid state.[12] These results prompted us to investigate other ROH species. Here we report the synthesis, crystal structures, electrochemical analysis, magnetic, and electron paramagnetic resonance (EPR) studies of the SCO systems $[Fe^{III}(bztpen)(OR)](PF_6)_2$ (**1-OR**) with R = methyl (**1-OMe**), ethyl (**1-OEt**), propyl (**1-OProp**), *n*-butyl (**1-OBut^n**), *i*-butyl (**1-OBut^i**), and ethylene glycoxide (**1-OEtg**).

RESULTS AND DISCUSSION

Synthesis. Crystalline samples of each alkoxide derivative were obtained using two different strategies depending on the solubility of bztpen and the Fe^{III} salt in the corresponding alcohol. The MeO^-, EtO^-, $PropO^-$, and $EtgO^-$ derivatives crystallized after slow evaporation of the resulting yellow-green solutions containing Fe^{III}/bztpen/PF_6^- (1:1:2) solubilized in the corresponding alcohol. Because of the high insolubility of the Fe^{III}/bztpen/PF_6^- mixture in *n*-butanol and isobutanol, this method was not appropriate to obtain the ^{n}ButO$^-$ and ^{i}ButO$^-$ derivatives. Thus, crystalline samples of **1-OBut^n** and **1-OBut^i** were obtained by layering acetone solutions of the precursor compound **1-OH** and the corresponding alcohols.

Crystal Structure. The crystal structures of **1-OEt**, **1-OProp**, **1-OBut^n**, **1-OBut^i**, and **1-OEtg** were investigated at 130 and 298 K. In all cases, the structures were found to be similar to the previously reported structure of $[Fe^{III}(bztpen)(OMe)](PF_6)_2$. Tables 1 and 2 respectively contain relevant crystallographic data and bond lengths and angles for the whole series of compounds. The data for the methanolate derivative have also been included for comparison. Figure 1 gathers the molecular structures for all of the compounds together with the corresponding atom-numbering schemes. The compounds display the orthorhombic *Pbca* space group at both temperatures. The iron atom is in a severely distorted octahedral $[FeN_5O]$ environment, wherein the five nitrogen atoms belong to the pentadentate bztpen ligand and the oxygen atom comes from the alkoxide group, which acts as a monodentate terminal ligand in all cases. Two PF_6^- anions balance the charge of the $[Fe^{III}(bztpen)(OR)]^{2+}$ species. The bztpen ligand coordinates the Fe^{III} atom, defining a distorted square pyramid in which the nitrogen atom N(2) lies on the axial apex. The opposite apex is occupied by O(1), thereby completing the octahedron. The N(2) atom is in the center of a tripod whose arms are defined by two picolylamine-type moieties [N(2)−C(7)−C(8)−N(3) and N(2)−C(6)− C(5)−N(1)] and an ethylenediamine-type moiety [N(2)−C(13)−C(14)−N(4)]. These arms are anchored to the iron atom through the atoms N(3), N(1), and N(4), respectively. An additional picolylamine-type arm, [N(4)−C(15)−C(16)−N(5)], originates at the N(4) atom and coordinates the remaining equatorial position of the Fe^{III} ion center through N(5). For the $[FeN_5]$ core, the average Fe−

Table 1. Crystallographic Data for 1-OMe, 1-OEt, 1-OProp, 1-OBut^n, 1-OBut^i, and 1-OEtg

	1-OMe		1-OEt		1-OProp		1-OBut^n		1-OBut^i		1-OEtg	
formula	$C_{28}H_{33}F_{12}FeN_5OP_2$		$C_{29}H_{34}F_{12}FeN_5OP_2$		$C_{30}H_{36}F_{12}FeN_5OP_2$		$C_{31}H_{38}F_{12}FeN_5OP_2$		$C_{31}H_{38}F_{12}FeN_5OP_2$		$C_{29}H_{34}F_{12}FeN_5O_2P_2$	
MW	801.38		814.4		828.43		842.45		842.45		830.4	
λ [Å]	0.71073		0.71073		1.54184		1.54184/0.71073		0. 71073		0.71073	
T [K]	100	298	130	298	130	298	130	298	130	298	130	298
space group	*Pbca*		*Pbca*		*Pbca*		*Pbca*		*Pbca*		*Pbca*	
a [Å]	17.0898(11)	17.4170(14)	17.8729(4)	17.9910(3)	17.9819(10)	18.3097(4)	18.3065(4)	18.4705(9)	18.2901(3)	18.5147(8)	17.9081(3)	18.0743(8)
b [Å]	19.1861(9)	19.224(2)	18.8767(4)	19.1695(13))	18.7660(7)	19.0793(5)	19.1694(5)	19.564(3)	18.8688(4)	19.2407(7)	18.9837(4)	19.2450(10)
c [Å]	19.3923(9)	19.7710(9)	19.5847(4)	19.9287(11)	19.7676(10)	20.1284(5)	19.7073(5)	19.9882(11)	19.7237(3)	20.0050(9)	19.4800(5)	19.7958(8)
V [Å^3]	6310.8(2)	6588.6(3)	6607.5(2)	6872.9(12)	6670.5(6)	7031.6(3)	6915.8(3)	7222.9(11)	6806.9(2)	7126.5(5)	6622.5(2)	6885.8(5)
Z	8		8		8		8		8		8	
ρ_{calc} [Mg m^{-3}]	1.674	1.608	1.637	1.574	1.650	1.565	1.618	1.549	1.644	1.570	1.666	1.602
μ [mm^{-1}]	0.680	0.653	0.660	0.630	5.472	5.191	5.288	0.602	0.639	0.611	0.658	0.633
R	0.0571	0.0957	0.0361	0.0735	0.0584	0.0598	0.0337	0.0547	0.0352	0.0611	0.0451	0.0673
wR_2	0.1274	0.2556	0.0967	0.1773	0.1137	0.1385	0.0889	0.1^{21}6	0.0800	0.1256	0.1103	0.1678

DOI: 10.1021/ic503081x
Inorg. Chem. XXXX, XXX, XXX−XXX

Table 2. Coordination Bond Lengths (Å) and Angles (deg) for 1-OMe, 1-OEt, 1-OProp, 1-OBu^n, 1-OBu^i, and 1-OEtg

	1-OMe		1-OEt		1-OProp		1-OBu^n		1-OBu^i		1-OEtg	
	100 K	298 K	130 K	298 K	130 K	298 K	130 K	298 K	130 K	298 K	130 K	298 K
Fe–N(1)	2.001(3)	2.095(12)	1.9750(18)	2.092(5)	1.961(3)	2.078(3)	1.9619(18)	2.045(3)	1.9631 (15)	2.048	1.973(2)	2.059(4)
Fe–N(2)	2.070(3)	2.209(9)	2.0384(17)	2.199(4)	2.032(2)	2.194(3)	2.0375(17)	2.167(3)	2.0359 (14)	2.162	2.029(2)	2.154(3)
Fe–N(3)	2.000(3)	2.105(11)	1.9727(18)	2.079(5)	1.971(3)	2.083(3)	1.9813(17)	2.057(3)	1.9768 (15)	2.057	1.980(2)	2.052(4)
Fe–N(4)	2.093(3)	2.224(10)	2.0574(17)	2.179(4)	2.042(2)	2.172(3)	2.0441(17)	2.142(3)	2.0452(14)	2.142	2.050(2)	2.147(3)
Fe–N(5)	2.026(3)	2.138(11)	1.9931(18)	2.127(5)	1.979(3)	2.125(3)	1.9809(18)	2.091(3)	1.9853 (15)	2.084	1.994(2)	2.084(4)
Fe–O(1)	1.793(3)	1.784(9)	1.8048(15)	1.790(4)	1.801(2)	1.782(3)	1.8005(15)	1.781(3)	1.8041(12)	1.793	1.810(2)	1.794(3)
$\langle FeN_5\rangle_{av}$	2.038	2.154	2.007	2.135	1.997	2.130	2.001	2.100	2.001	2.099	2.005	2.099
$\langle FeN_5O\rangle_{av}$	1.997	2.092	1.973	2.078	1.964	2.072	1.968	2.047	1.968	2.048	1.973	2.048
$\Delta[FeN_5]$		0.116		0.128		0.133		0.099		0.098		0.094
$\Delta[FeN_5O]$		0.095		0.105		0.108		0.079		0.080		0.075
Fe–O(1)–C(28)	129.9(3)	153.9(12)	126.79(15)	150.1(9)	128.12(18)	151.5(6)	128.77(14)	148.3(6)	127.36(11)	134.5(3)	127.22(18)	134.9(4)
Δ[Fe–O(1)–C(28)]		24		23.3		23.4		19.6		7.1		7.7
Σ [deg]	60.47	88.60	51.62	80.80	49.53	78.29	49.41	73.81	49.99	74.25	50.14	72.97
$\Delta\Sigma$ [deg]		28.13		29.18		28.76		24.40		24.26		22.83
Φ [deg]	5.34	6.06	4.25	5.15	4.07	4.90	4.16	4.83	3.87	4.57	4.19	4.81
$\Delta\Phi$ [deg]		0.72		0.90		0.83		0.67		0.70		0.62

N bond length at 100 K is in the range $\langle FeN_5\rangle_{av}$ = 2.038−1.997 Å and increases to 2.154−2.095 Å at 298 K, involving a bond length increase in the 0.094−0.133 Å range. Contrarily, for the oxygen atom the low-temperature (LT) structures show slightly larger Fe−O(1) bonds (1.793−1.810 Å) than the high-temperature (HT) structures (1.782−1.789 Å), a fact that makes less pronounced the overall change of the average bond length of the octahedron, $\Delta[FeN_5O]$, which was found to be in the 0.069−0.095 Å range (Table 2).

The sum of the deviations from the ideal octahedron of the 12 "cis" N−Fe−N angles θ ($\Sigma = \sum_{i=1}^{12} |\theta_i - 90°|$) shows that the coordination center is strongly distorted in the LT structure, with the Σ value in the interval 49−61°. Furthermore, this distortion increases on average by ca. 32% to 73−88° for the HT structures (Table 2). In contrast, the average of the 24 trigonal distortion angles Φ defined by superposition of two opposite triangles of the octahedron ($\Phi = \sum_{i=1}^{24} |\phi_i - 60|/24$) and its change with temperature were estimated to be very small [0.82−1.13° (LT) and 1.44−1.87° (HT)]. Interestingly, theFe−O(1)−C(28) angle is quite sensitive to temperature variation, as it increases by 24°, 23.3°, 23.4°, 19.6°, 7.1°, and 7.7° for **1-OMe**, **1-OEt**, **1-OProp**, **1-OBu^n**, **1-OBu^i**, and **1-OEtg**, respectively, upon moving from the LT structure to the HT structure.

Two perspective views of the crystal packing seen in the [010] and [010] directions are shown in Figure 2 for **1-OBu^n** as a representative for the whole family here reported. The cation complexes stack in the [010] direction, determining the shortest $Fe^{III}\cdots Fe^{III}$ distance of 9.7198(5) Å at 130 K. A complete list of $Fe^{III}\cdots Fe^{III}$ intermolecular distances for the LT structures of the title compounds is given in Table 3. In the LT crystal packing, the cationic molecules interact directly with each other through weak C···C intermolecular contacts, defining a three-dimensional network. Most of these contacts are in the 3.6−3.7 Å interval. Furthermore, these interactions are reinforced by a number of C···F cation−anion contacts. Tables S1 and S2 in the Supporting Information gather the intermolecular distances smaller than the sum of the van der Waals radii (C···C, 3.7 Å; C···F, 3.20 Å).

Magnetic and Thermodynamic Properties. The thermal dependence of the $\chi_M T$ product, where χ_M is the magnetic susceptibility per mole of compound and T is the temperature, is displayed in Figure 3 for **1-OEt**, **1-OProp**, **1-OBu^n**, **1-OBu^i**, and **1-OEtg** together with that of a new sample of the previously reported derivative **1-OMe**.[12] The $\chi_M T$ product is 4.15 cm^3 K mol^{-1} for **1-OMe** at 350 K and 4.00 cm^3 K mol^{-1} for **1-OEt**, 3.98 cm^3 K mol^{-1} for **1-OProp**, 3.81 cm^3 K mol^{-1} for **1-OBu^n**, 3.98 cm^3 K mol^{-1} for **1-OBu^i**, and 3.95 cm^3 K mol^{-1} for **1-OEtg** at 400 K. These values are slightly lower than expected for an Fe^{III} ion in the HS state ($^6A_2$, $S = {}^5/_2$), 4.37 cm^3 K mol^{-1} (g = 2.00). Then $\chi_M T$ progressively decreases upon cooling to reach constant values in the interval 0.70−0.82 cm^3 K mol^{-1}. These values are slightly higher than the value of about 0.5 cm^3 K mol^{-1} usually found for an Fe^{III} ion in the LS state (formally $^2T_2$, $S = {}^1/_2$). This behavior clearly indicates the occurrence of an almost complete LS−HS spin-state conversion. The heating mode matches perfectly the cooling mode, a fact that indicates the lack of thermal hysteresis for all of the derivatives.

To analyze these SCO behaviors, we simulated the $\chi_M T$ versus T curves using a modification[13] of the regular-solution model proposed by Slichter and Drickamer[14] in the context of the SCO phenomenon:

DOI: 10.1021/ic503081x
Inorg. Chem. XXXX, XXX, XXX−XXX

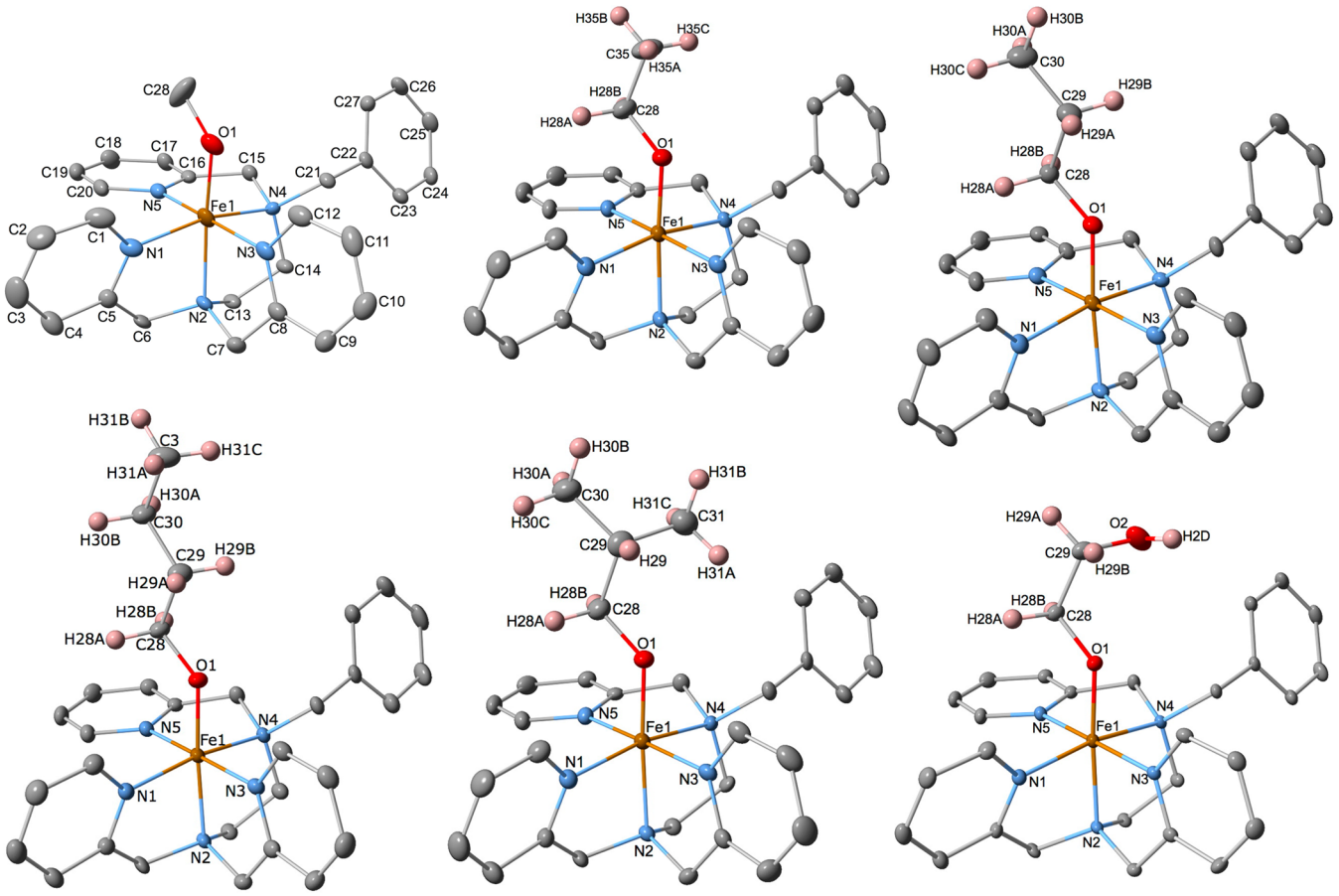

Figure 1. ORTEP representations of **1-OMe**, **1-OEt**, **1-OProp**, **1-OBut^n**, **1-OBut^i**, and **1-OEtg** in the LS state. Hydrogen atoms have been shown only for the alkoxide ligands for the sake of simplicity. The atom numbering of the bztpen ligand is the same for all of the derivatives. Thermal ellipsoids are presented at 40% probability.

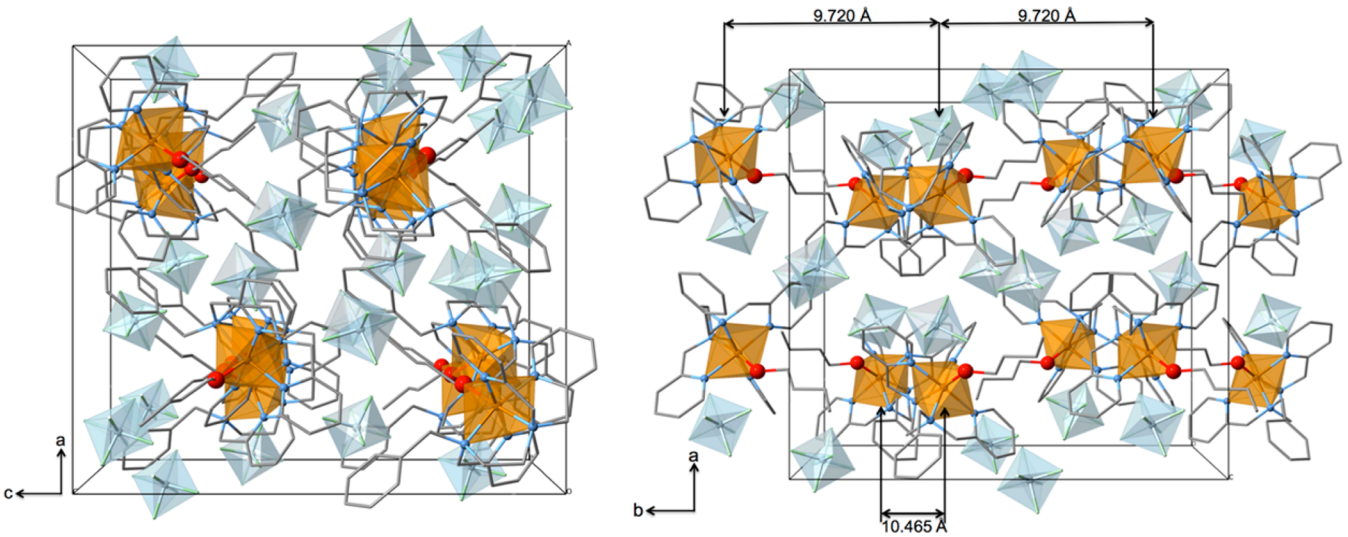

Figure 2. Two orthogonal views of the crystal packing of **1-OBut^n** (130 K).

$$\ln\left[\frac{1-\gamma_{HS}}{\gamma_{HS}-f_{HS}}\right] = \frac{\Delta H + \Gamma(1+f_{HS}-2\gamma_{HS})}{RT} - \frac{\Delta S}{R} \quad (1)$$

where γ_{HS} is the HS mole fraction, f_{HS} is the residual HS mole fraction of species that do not show SCO at low temperature, ΔH and ΔS are, respectively, the enthalpy and entropy variations during the SCO, Γ represents the interaction energy between molecules (cooperativity), and R is the gas constant. The quantities γ_{HS} and f_{HS} can be expressed as functions of the $\chi_M T$ product as follows:

$$\gamma_{HS} = \frac{(\chi_M T)_m - (\chi_M T)_{LS}}{(\chi_M T)_{HS} - (\chi_M T)_{LS}} \quad (2)$$

DOI: 10.1021/ic503081x
Inorg. Chem. XXXX, XXX, XXX−XXX

Table 3. $Fe^{III}\cdots Fe^{III}$ Intermolecular Distances for the LT Crystal Structures

1-OMe	1−EtO	1-OProp	1-OBut^{n}	1-OBut^{i}	1-OEtg
9.3969(5)^{i}	9.6209(5)^{ii}	9.5405(9)^{v}	9.7198(5)^{v}	9.5934(6)^{v}	9.6343(6)^{v}
9.8283(4)^{ii}	9.7469(5)^{i}	9.7697(7)^{i}	9.9458(5)^{vi}	9.8790(6)^{viii}	9.8064(5)^{viii}
10.5819(5)^{iii}	10.5113(4)^{iv}	10.5300(8)^{iii}	10.4646(5)^{vii}	10.5745(5)^{iii}	10.4438(6)^{iii}

$^{i}x-{}^{1}/_{2}, y, -z+{}^{3}/_{2}$. $^{ii}-x+{}^{3}/_{2}, y-{}^{1}/_{2}, z$. $^{iii}x, -y+{}^{1}/_{2}, z+{}^{1}/_{2}$. $^{iv}x, -y+{}^{3}/_{2}, z-{}^{1}/_{2}$. $^{v}-x+{}^{1}/_{2}, y+{}^{1}/_{2}, z$. $^{vi}-x+1, y, -z+{}^{3}/_{2}$. $^{vii}x, -y+{}^{1}/_{2}, z-{}^{1}/_{2}$. $^{viii}x+{}^{1}/_{2}, y, -z+{}^{1}/_{2}$.

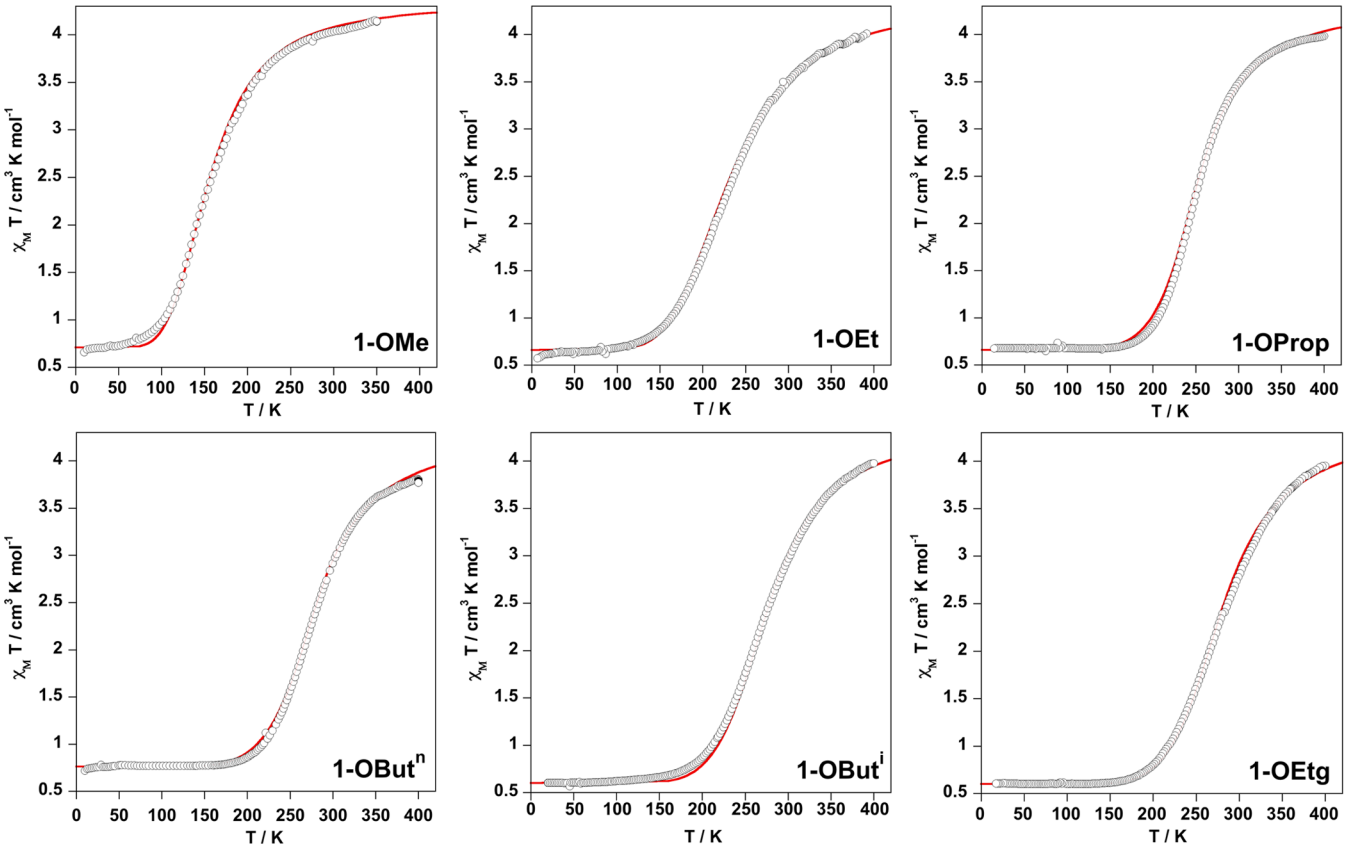

Figure 3. Experimental (open circles) and simulated (red line) $\chi_M T$ vs T plots for **1-OMe**, **1-OEt**, **1-OProp**, **1-OBut^{n}**, **1-OBut^{i}**, and **1-OEtg**.

Table 4. Thermodynamic Parameters Obtained from Simulations of $\chi_M T$ versus T curves for 1-OMe, 1-OEt, 1-OProp, 1-OBut^{n}, 1-OBut^{i}, and 1-OEtg, Along with Acidity Constants (pK_a) and Ionization Potentials (IP) of the Corresponding Alcohols HOR (See the Text)

	1-OMe	1-OEt	1-OProp	1-OBut^{n}	1-OBut^{i}	1-OEtg
ΔS (J K^{-1} mol^{-1})	43.0	45.0	43.0	40.0	48.0	47.0
ΔH (kJ mol^{-1})	6.79	10.53	10.96	11.36	13.34	13.25
Γ (kJ mol^{-1})	0.00	0.00	1.80	2.2	1.3	1.4
$T_{1/2}$ (K)	158.0	234.0	255.0	284.0	278	282
$(\chi_M T)_R$ (cm^3 K mol^{-1})	0.71	0.64	0.67	0.77	0.61	0.60
% LS (300 K)^{a}	8.7	22.3	23.1	37.6	36.8	40.6
pK_a^{b}	15.8	16.5	16.8	16.9	17.3	14.8
IP (eV)^{c}	10.84	10.47	10.15	10.04	10.12	10.16

^{a}Estimated from $\chi_M T$ at 300 K using $(\chi_M T)_{LS}$ = 0.5 cm^3 K mol^{-1} and $(\chi_M T)_{HS}$ = 4.375 cm^3 K mol^{-1}. ^{b}Taken from ref 19. ^{c}Taken from ref 28.

$$f_{HS} = \frac{(\chi_M T)_R - (\chi_M T)_{LS}}{(\chi_M T)_{HS} - (\chi_M T)_{LS}} \quad (3)$$

where $(\chi_M T)_m$ represents the $\chi_M T$ value at any temperature, $(\chi_M T)_R$ corresponds to the residual value due to HS Fe^{III} species at low temperatures, and $(\chi_M T)_{HS}$ and $(\chi_M T)_{LS}$ represent the $\chi_M T$ values of the 100%-populated HS and LS species, respectively. The latter two quantities were taken as fixed parameters with values equal to 4.37 and 0.5 cm^3 K mol^{-1} respectively, while $(\chi_M T)_R$, $T_{1/2} = \Delta H/\Delta S$, Γ, and ΔS were considered as adjustable parameters. As can be seen in Figure 3, the experimental (open circles) and calculated (red line) $\chi_M T$ versus T plots agree satisfactorily for all of the compounds. The corresponding thermodynamic parameters are listed in Table 4. The $(\chi_M T)_R$ values found in the interval 0.6−0.8 cm^3 K mol^{-1}

DOI: 10.1021/ic503081x
Inorg. Chem. XXXX, XXX, XXX−XXX

denote the presence of about 4% residual HS centers at low temperatures.

Electron Paramagnetic Resonance Spectroscopy. EPR spectroscopy has been used since long ago to characterize the electronic states involved in the SCO of Fe^{III} complexes.[15] In this work, we recorded the EPR spectra for all of the derivatives in the temperature interval 300−50 K. Figure 4 displays the

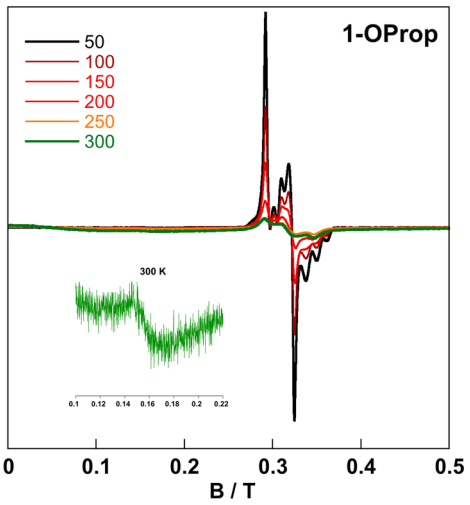

Figure 4. EPR spectra of **1-OProp** in the temperature interval 50−300 K. The inset corresponds to the magnification of the spectrum at 300 K in the field region 0.14−0.16 T ($g \approx 4.47$).

EPR spectra of **1-OProp** as a representative example, and the remaining spectra are shown in Figure S1 in the Supporting Information. At 300 K, two weak signals are observed in the EPR spectrum, a broad one at $g \approx 4.47$ (particularly well visible for **1-OMe**, **1-OEt**, and **1-OBu^n**) and a more intense one centered at $g \approx 2.10$. As the temperature is decreased, the former signal, assignable to Fe^{III} in the HS state, practically disappears at the expense of the second rhombic signal characteristic of LS Fe^{III}, which increases significantly, thereby confirming the HS−LS transformation. At 50 K, where the complexes are essentially in the LS state, the estimated g values were found to be in the intervals $g_1 = 1.91-2.04$, $g_2 = 2.08-2.11$, and $g_3 = 2.28-2.32$ (Table S3 in the Supporting Information). All of the derivatives except for **1-OMe** and **1-OBu^n** display superhyperfine coupling between the electron spin of Fe^{III} and the nuclear spin of ^{14}N ($I = 1$). In the particular case of **1-OProp**, a superhyperfine coupling parameter of 120 G could be estimated from a reasonably good simulation.[16]

Electrochemistry. In order to test the stability of the title compounds in solution, cyclic voltammograms were recorded for **1-OMe**, **1-OEt**, **1-OProp**, and **1-OBu^n** (Figure 5). The potential peak values of the corresponding redox signals are gathered in Table 5. The electrochemical behavior of all of the compounds shows an irreversible signal with a small shoulder for the reduction of Fe(III) to Fe(II) around to −0.2 to −0.4 V vs Fc^+/Fc (the E_{cp1} and E_{cp2} peaks). When the scan potential was inverted, three oxidation signals were observed in the −0.4 to 0.5 V vs Fc^+/Fc interval (the E_{ap2}, E_{ap3}, and E_{ap4} peaks; see Figure 5). However, the potential peak values for the four investigated compounds were very similar and showed no significant differences (Figure 5 inset). These facts can be associated with predominant electronic effects, namely, the

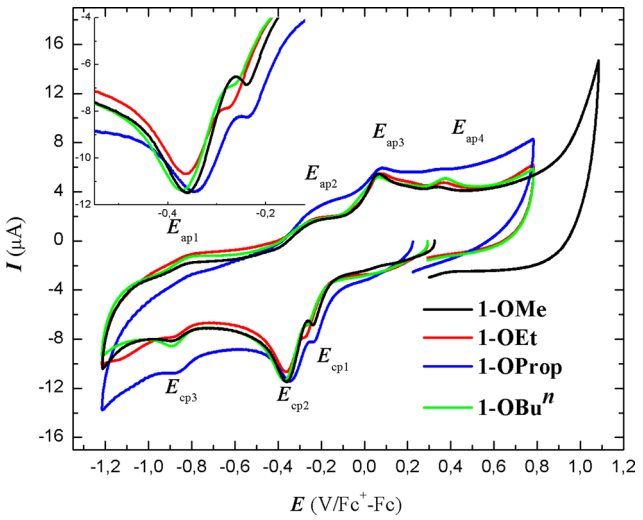

Figure 5. Typical cyclic voltammograms at 100 mV s^{-1} obtained in the cathodic direction in 0.1 M $(C_4H_9)_4NPF_6$ acetone solution on a glassy carbon electrode (ϕ = 3 mm internal diameter), employing a pseudoreference electrode of Ag/AgCl(s) in 0.1 M $(C_4H_9)_4NCl$ acetone solution and a platinum counter electrode in 0.1 M $(C_4H_9)_4NPF_6$ acetone solution, for the four iron(III) compounds **1-OMe** (black), **1-OEt** (red), **1-OProp** (blue), and **1-OBu^n** (green).

Table 5. Potential Peak Values (in V vs Fc^+/Fc) of 1-OMe, 1-OEt, 1-OProp, and 1-OBu^n Obtained for Cathodic (E_{cp}) and Anodic (E_{ap}) Processes in Acetone Solutions on a Glassy Carbon Electrode

compound	E_{cp1}	E_{cp2}	E_{ap2}	E_{ap3}	E_{ap4}
1-OMe	−0.235	−0.359	−0.246	0.067	0.341
1-OEt	−0.275	−0.361	−0.245	0.073	0.371
1-OProp	−0.234	−0.342	−0.259	0.076	0.341
1-OBu^n	−0.264	−0.371	−0.234	0.065	0.373

hard-base character of the RO^- anion, which strongly stabilizes the Fe^{III} oxidation state. From the observed electrochemical behavior, it can be asserted that the reduced species are very unstable. Consequently, all attempts to obtain the reduced species in solution for any of these compounds were fruitless.

DISCUSSION

Multidentate tri-, tetra-, and hexadentate Schiff base-type ligands with donor atoms N_2O, N_2O_2, and N_4O_2, respectively, represent the most important source of iron(III) SCO complexes, with $[FeN_4O_2]$ as their common coordination environment. They usually combine imino and amino N-donor groups with more basic enolate or phenolate O-donor groups that provide stabilization of the ferric oxidation state as well as the appropriate ligand field strength to induce spin crossover behavior. In contrast, the pentaaza ligand bztpen with one ethylenediamine and three pyridine moieties is a priori more prone to stabilize the Fe^{II} oxidation state, although it also may form stable Fe^{III} complexes. In this respect, **1-OMe** was obtained from spontaneous oxidation of $[Fe^{II}(bztpen)(MeOH)]^{2+}$ in methanol and subsequent deprotonation of the coordinated methanol molecule to give the methoxide complex. However, the remaining members of this series were synthesized directly from solution of $[Fe(bztpen)]^{3+}$ in the presence of the appropriate alcohol. As far as we know, these derivatives represent the first members of a family of solid-state

DOI: 10.1021/ic503081x
Inorg. Chem. XXXX, XXX, XXX−XXX

SCO Fe^{III} complexes that display both an $[FeN_5O]$ coordination sphere and strongly basic anionic alkoxide ligands as the O donors.

The SCO behavior of the title compounds has been investigated by means of thermal variation of the magnetic susceptibility and the EPR spectrum. The EPR spectrum is characteristic of Schiff base Fe^{III} SCO complexes.[3] The thermal dependence of $\chi_M T$ follows reasonably well the Gibbs−Boltzmann law described by regular-solution theory in the version of the Slichter−Drickamer expression.[13,14] This mean-field theory also provides an objective criterion to evaluate cooperativeness as the ratio $C = \Gamma/2RT_{1/2}$. Strong cooperative SCO occurs for $C \geq 1$ while poor cooperative transitions are observed for $C \leq 1$. The spin-state transformation extends more than 200 K for all of the derivatives, denoting the occurrence of poor cooperativity. Consistently, the estimated Γ parameters were found in the interval 0−2.2 kJ mol^{-1} with C values equal to 0 for **1-OMe** and **1-OEt** and 0.42, 0.46, 0.28, and 0.30 for **1-OProp**, **1-OBut^n**, **1-OBut^i**, and **1-OEtg**, respectively. It deserves to be stressed that qualitative estimation of the relative cooperativity of two SCO behaviors from visual comparison of the steepness of the SCO curves is an acceptable method only when their $T_{1/2}$ temperatures are similar. This explains why **1-OMe** and **1-OProp** displaying similar steepnesses have such different C values.

Cooperativity, which mainly arises from elastic interactions, is a measure of how efficiently the intramolecular changes associated with the SCO are transmitted through intermolecular interactions from one active center to another active center in the crystal. In this respect, significant variation of the bond angles of the $[FeN_5O]$ coordination core are observed. The parameter Σ is large for both the LT and HT structures, indicating severe distortion of the Fe^{III} octahedron in the LS and HS states. However, Σ is smaller for the LT structure, as shown by the difference $\Delta\Sigma = \Sigma_{HT} - \Sigma_{LT} \approx 20-30°$. It is worth mentioning that at 300 K, where the crystal structures of the title compounds were measured, the conversion of the LS state to the HS state is not complete (see Table 3). Extrapolation of $\Delta[FeN_5]$ to 100% HS species gives values in the interval 0.12−0.16 Å. These values compare well with the $\Delta[FeN_4]$ values observed for most Schiff base-type ligands.[3,11,17] The most important difference with respect to the latter family is the negative variation of the Fe−O bond in moving from the LS state to the HS state (extrapolated to 100% HS, this is in the interval 0.01−0.03 Å), a fact that mitigates the total variation of the average bond length of the $[FeN_5O]$ coordination core. Apparently, despite the large number of intermolecular contacts, either direct between complex cations or mediated through the anions (see Tables S1 and S2 in the Supporting Information), all of these structural changes are smoothly accommodated in the crystal lattice.

The ΔS values estimated from simulation of the magnetic curves are in the interval 40−48 J K^{-1} mol^{-1}. These values exceed the pure electronic spin contribution $R\ln(6/2) = 9.13$ J K^{-1} mol^{-1} resulting from the difference in the spin degeneracies of the HS and LS states of the ferric complex (considering the orbital contribution of the LS state to be completely removed for symmetry reasons). The phonon entropy and a small contribution from the structure change account for the main part of the remaining entropy.

Differential scanning calorimetry (DSC) is the common technique to measure the excess heat capacity (ΔC_p) that enables evaluation of the ΔH and ΔS values associated with the SCO. However, as happens for most Fe^{III} SCO complexes, the poor cooperativity displayed by the title compounds prevented the direct measurement of the thermal dependence of ΔC_p. Instead, simulation of the thermal dependence of $\chi_M T$ using the Slichter−Drickamer model afforded reasonable thermodynamic parameters. In this respect, only a reduced number of DSC studies have been carried out for Fe^{III} SCO complexes.[18] From these studies, the obtained ΔS values were found to be in the 16−27 J K^{-1} mol^{-1} interval for a series of Fe^{III}−thiosemicarbazone complexes with $[FeN_2O_2S_2]$ cores,[18a,d,f] while for the most investigated Schiff base ferric complexes with $[FeN_4O_2]$ cores, ΔS is in the range 34−41 J K^{-1} mol^{-1}.[18b,c,e] The unusually low ΔS values found for complete SCO in the Fe^{III}−thiosemicarbazone complexes has been associated with the nature of the coordination core.[18d] The estimated ΔS values for the title compounds (43−48 J K^{-1} mol^{-1}; see Table 4) are in the upper limit of the interval obtained from DSC measurements for a series of Schiff base ferric SCO complexes.

The observed $T_{1/2}$ values increase along the series **1-OMe**, **1-OEt**, **1-OProp**, and **1-OBut^n**, a fact that suggests an increase in σ-donor capacity of the alkoxide group as the length of the alkyl chain increases, thereby indicating enhancement of the ligand field strength felt by the Fe^{III} ion and hence stabilization of the LS state. Indeed, the moderate increase in the pK_a values of the corresponding alcohols parallels the increase in $T_{1/2}$ for the series (Table 4).[19] Nevertheless, **1-OEtg** represents an important exception to this trend since it displays the smallest pK_a value of the series and $T_{1/2}$ = 282 K. The larger acidity of the ethylene glycol could be related to its capability to form intramolecular hydrogen bonding, making it easier for the first proton to ionize. The slightly smaller $T_{1/2}$ value shown by **1-OBut^i** with respect to that of **1-OBut^n** could be the result of fine-tuning of the ligand field strength derived from differences in the crystal packing of the two derivatives.

A much better general correlation has been found between $T_{1/2}$ and the ionization potential (IP) in the gas phase of the corresponding alcohol H**OR** of the series, with $T_{1/2}$ increasing as the IP decreases (see Table 4). The first ionization takes place on the nonbonded electrons of the O atom and gives an idea of the molecular electronegativity of H**OR** and hence of the donor capability of the corresponding alkoxide.[20] Apparently, intramolecular hydrogen bonding in the ethylene glycol molecule in the gas phase seems not to affect its IP value significantly, and consequently, a good $T_{1/2}$−IP correlation is also observed for **1-OEtg**.

Finally, the spin crossover change centered near room temperature makes **1-OBut^n**, **1-OBut^n**, and **1-OEtg** very attractive materials for device fabrication, e.g., for thermometry applications.[21]

CONCLUSION

We have reported for the first time a family of alkoxide Fe^{III} SCO complexes. The complexes display the $[FeN_5O]$ coordination core made up of the pentadentate N-donor ligand bztpen and a series of alkoxide anions as O-donor ligands. The crystal and molecular structures have been investigated at two representative temperatures where the HS and LS species predominate. The spin crossover properties have been monitored by means of the thermal variation of the magnetic susceptibility and the EPR spectra. The gradual SCO behavior observed for all of derivatives has been rationalized in

DOI: 10.1021/ic503081x
Inorg. Chem. XXXX, XXX, XXX−XXX

terms of the crystal structure and the Schlichter−Drickamer model, and reasonably good thermodynamic parameters have been obtained. The observed change in $T_{1/2}$ can be explained in terms of the basicity of the alkoxide and hence in terms of the ligand field strength that the alkoxide imparts to the Fe^{III} ion. The electrochemistry of these complexes in solution shows that the Fe(II) oxidation state for all of the complexes is very unstable.

EXPERIMENTAL SECTION

Materials. Commercially available materials were used without further purification. $[Fe^{III}(DMSO)_6](PF_6)_3$ and bztpen were synthesized according to published procedures.[22,8b]

Synthesis of the Precursor [Fe(bztpen)OH](PF$_6$)$_2$ (1-OH). To an aqueous solution of $[Fe(DMSO)_6](NO_3)_3$ (5 mL, 0.213 g, 0.3 mmol) was added an acetone solution of bztpen (5 mL, 0.127 g, 0.30 mmol) under constant stirring. The resulting red-brown solution was heated at about 70 °C to evaporate the acetone. Then an aqueous solution of NH_4PF_6 (5 mL, 0.245 g, 1.5 mmol) was added to the concentrated solution under constant stirring, and a light-yellow-beige solid was formed immediately. A bright-yellow microcrystalline solid was obtained after filtering and washing with small portions of acetone and water. Yield: 0.218 g, 92.4%. Yellow powder. FAB MS: m/z 496 $(M - 2PF_6^- + e^-)^+$, m/z 498 $(M - 2PF_6^- - OH^- + H_2O + H^+ + 3e^-)^+$, m/z 514 $(M - 2PF_6^- + H_2O + e^-)^+$. Anal. Calcd for $C_{27}H_{30}N_5OF_{12}P_2Fe$ (786.56 g/mol): C, 41.24; N, 8.91; H, 3.85. Found: C, 41.52; N, 8.78; H, 3.83%.

Synthesis of the Complexes 1-OR. Method I: Samples constituted of single crystals of **1-OR** were obtained in reasonably good yields by slow liquid−liquid diffusion of **1-OH** dissolved in acetone and the corresponding alcohol (1:3 respectively). Method II: **1-OMe**, **1-OEt**, **1-OProp**, and **1-OEtg** were alternatively obtained by direct synthesis, mixing solutions of $Fe(NO_3)_3{\cdot}9H_2O$ (0.168 g, 0.24 mmol) and the ligand bztpen (0.100 g, 0.24 mmol) solubilized in appropriate amounts of the corresponding alcohol. After addition of a solution of NH_4PF_6 (0.154 g, 0.95 mmol) in the same alcohol and slow evaporation, the crystalline compounds were obtained in even better yield than using the former method. The crystals were filtered and washed with cold water and allowed to dry in the open air.

1-OMe. Yields: 0.009 g, 90 % (method I); 0.170 g, 90% (method II). Green crystals. Anal. Calcd for $C_{28}H_{32}N_5OF_{12}P_2Fe$ (800.37 g/mol): C, 42.02; N, 8.75; H, 4.03. Found: C, 41.89; N, 8.86; H, 4.12%.

1-OEt. Yield, 0.009 g, 90 % (method I), 0.173 g, 90% (method II). Green crystals. FAB MS: m/z 496 $(M - 2PF_6^- - CH_2CH_3^+ + H^+ + e^-)^+$, m/z 498 $(M - 2PF_6^- - OCH_2CH_3^- + H_2O + H^+ + 3e^-)^+$, m/z 514 $(M - 2PF_6^- - CH_2CH_3^+ + H_2O + H^+ + e^-)^+$, m/z 524 $(M - 2PF_6^- + e^-)^+$. Anal. Calcd for $C_{29}H_{34}N_5OF_{12}P_2Fe$ (814.40 g/mol): C, 42.77; N, 8.60; H, 4.21. Found: C, 43.17; N, 8.86; H, 4.08%.

1-OProp. Yield: 0.006 g, 60% (method I), 0.137 g, 70% (method II). Green crystals. FAB MS: m/z 496 $(M - 2PF_6^- - CH_2CH_2CH_3^+ + H^+ + e^-)^+$, m/z 498 $(M - 2PF_6^- - OCH_2CH_2CH_3^- + H_2O + H^+ + 3e^-)^+$, m/z 557 $(M - 2PF_6^- + H_2O + H^+ + 2e^-)^+$, m/z 631 $(M - PF_6^- - OH^- - 2H_2O + H^+ + 2e^-)^+$, m/z 651 $(M - PF_6^- - CH_3^+ - H_2O + H^+)^+$. Anal. Calcd for $C_{30}H_{36}N_5OF_{12}P_2Fe$ (828.56 g/mol): C, 43.50; N, 8.45; H, 4.38. Found: C, 43.62; N, 8.60; H, 3.98%.

1-OBu^n. Yield: 0.006 g, 60% (method I). Green crystals. FAB MS: FAB MS: m/z 496 $(M - 2PF_6^- - CH_2CH_2CH_2CH_3^+ + H^+ + e^-)^+$, m/z 498 $(M - 2PF_6^- - OCH_2CH_2CH_2CH_3^- + H_2O + H^+ + 3e^-)^+$, m/z 552 $(M - 2PF_6^- + e^-)^+$, m/z 571 $(M - 2PF_6^- + H_2O + H^+ + 2e^-)^+$, m/z 631 $(M - PF_6^- - HOCH_2^+ - 2H_2O + H^+)^+$, m/z 651 $(M - PF_6^- - CH_2CH_3^+ - H_2O + H^+)^+$. Anal. Calcd for $C_{31}H_{38}N_5OF_{12}P_2Fe$ (842.45 g/mol): C, 44.20; N, 8.31; H, 4.55. Found: C, 44.25; N, 8.66; H, 3.92%.

1-OBu^i. Yield: 0.006 g, 60% (method I). Green crystals. FAB MS: m/z 496 $(M - 2PF_6^- - CH_2CH(CH_3)_2^+ + H^+ + e^-)^+$, m/z 498 $(M - 2PF_6^- - OCH_2CH(CH_3)_2^- + H_2O + H^+ + 3e^-)^+$, m/z 552 $(M - 2PF_6^- + e^-)^+$, m/z 571 $(M - 2PF_6^- + H_2O + H^+ + 2e^-)^+$, m/z 631 $(M - PF_6^- - HOCH_2^+ - 2H_2O + H^+)^+$, m/z 651 $(M - PF_6^- - CH_2CH_3^+ - H_2O + H^+)^+$. Anal. Calcd for $C_{31}H_{38}N_5OF_{12}P_2Fe$ (842.45 g/mol): C, 44.20; N, 8.31; H, 4.55. Found: C, 44.28; N, 8.29; H, 3.96%.

1-OEtg. Yield: 0.006 g, 60 % (method I), 0.117 g, 60% (method II). Green crystals. Anal. Calcd for $C_{29}H_{34}N_5O_2F_{12}P_2Fe$ (830.40 g/mol): C, 41.89; N, 8.42; H, 4.24. Found: C, 41.47; N, 8.17; H, 3.17%.

Physical Measurements. Variable-temperature magnetic susceptibility measurements were carried out on samples constituted by small crystals of all complexes (15−20 mg) using a Quantum Design MPMS2 SQUID susceptometer equipped with a 5.5 T magnet and operating at 1 T and 1.8−400 K. Experimental susceptibilities were corrected for diamagnetism of the constituent atoms by the use of Pascal's constants. Variable-temperature EPR spectra were recorded on microcrystalline samples using a Bruker ELEXYS E580 spectrometer equipped with Bruker standard resonators for the X and Q bands. Data were collected at 50, 100, 150, 200, 250, and 300 K in the 20−9980.0 G field range with the following parameters: frequency = 9.472 GHz, power = 1.992 mW, power attenuation = 20.0 dB, modulation frequency = 100.00 kHz, modulation amplitude = 1.000 G, gain = 60 dB.

Single-Crystal X-ray Diffraction. The crystals of the $[Fe^{III}(bztpen)(OR)](PF_6)_2$ compounds were studied with an Oxford Diffraction Gemini "A" diffractometer with a CCD area detector using graphite-monochromatized Mo Kα radiation (λ = 0.71073 Å) for **1-OEt**, **1-OBu^n**, **1-OBu^i**, and **1-OEtg** and Cu Kα radiation (λ = 1.5418 Å) for **1-OProp** and **1-OBu^n** at 298 and 130 K. All of the crystals changed color from yellow to dark green as the temperature decreased. The CrysAlisPro and CrysAlis RED software packages[23] were used for data collection and data integration. The double-pass method of scanning was used to exclude any noise. The collected frames were integrated using an orientation matrix determined from the narrow-frame scans. Final cell constants were determined by global refinement; collected data were corrected for absorbance using analytical numeric absorption correction[24] on the basis of a multifaceted crystal model based on expressions for the Laue symmetry using equivalent reflections.

The following programs were used: SHELXS97 and SHELXL97[25] for structure solution and refinement; ORTEP-3 for Windows[26] for molecular graphics; and WinGX version 1.80.05[27] to prepare material for publication.

Full-matrix least-squares refinement was carried out by minimizing $(F_o^2 - F_c^2)^2$. All non-hydrogen atoms were refined anisotropically. For **1-OEtg**, the H atom of the hydroxyl group (H−O) was located in a difference map and refined isotropically with $U_{iso}(H) = 1.5$. For **1-OEt**, **1-OProp**, **1-OBu^n**, **1-OBu^i**, and **1-OEtg**, the H atoms attached to C atoms were placed in geometrically idealized positions and refined as riding on their parent atoms, with C−H = 0.93−0.99 Å and $U_{iso}(H) = 1.2U_{eq}(C)$ for aromatic and methylene groups and $U_{iso}(H) = 1.5U_{eq}(C)$ for methyl groups.

Electrochemistry. Electrochemical measurements were carried out using a potentiostat galvanostat (PAR 263-A) with a three-electrode system in 0.1 M $(C_4H_9)_4NPF_6$ acetone solution as the supporting electrolyte. A glassy carbon disk (0.071 cm^2) was used as the working electrode, a Pt wire as the auxiliary electrode, and 0.1 M $(C_4H_9)_4Cl$/AgCl(s)/Ag acetone solution as the reference electrode. The working electrode (C) was polished with alumina to ensure the absence of residues on the surface. All of the voltammograms were initiated from the null current potential ($E_{i=0}$), and the scan was initiated in both the positive and negative potential directions. In order to report the potentials used according to the IUPAC convention, voltammograms were obtained for an approximately 10^{-3} M solution of ferrocene (Fc) in a supporting electrolyte. For the working conditions, the electroactive domain was between −1.726 and 0.274 V vs Fc^+/Fc. In view of the irreversible nature of the studied systems, only the reduction peak potential values (Fe^{III} to Fe^{II}), were included as the characteristic potential values.

DOI: 10.1021/ic503081x
Inorg. Chem. XXXX, XXX, XXX−XXX

■ ASSOCIATED CONTENT

Supporting Information

Intermolecular C···C and F···C distances (Tables S1 and S2); EPR spectra in the temperature range 50−300 K (Figure S1); estimated *g* values (Table S3); and crystallographic data in CIF format for **1-OEt**, **1-OProp**, **1-OBu^n**, **1-OBu^i**, and **1-OEtg** at 130 and 298 K. This material is available free of charge via the Internet at http://pubs.acs.org.

■ AUTHOR INFORMATION

Corresponding Authors

*E-mail: vmus@unam.mx.

*E-mail: jose.a.real@uv.es.

Notes

The authors declare no competing financial interest.

■ ACKNOWLEDGMENTS

This work was supported by the Spanish Ministerio de Economía y Competitividad (MINECO) and FEDER funds (CTQ2013-46275-P) and Generalitat Valenciana (PROMETEO/2012/049). L.P.-L. thanks the Generalitat Valenciana and Universitat de València for a predoctoral fellowship.

■ REFERENCES

(1) For example, see: (a) Goodwin, H. A. *Coord. Chem. Rev.* **1976**, *18*, 293−325. (b) Gütlich, P. *Struct. Bonding (Berlin)* **1981**, *44*, 83−195. (c) König, E.; Ritter, G.; Kulshreshtha, S. K. *Chem. Rev.* **1985**, *85*, 219−234. (d) Hauser, A. *Comments Inorg. Chem.* **1995**, *17*, 17−40. (e) König, E. *Struct. Bonding (Berlin)* **1991**, *76*, 51−152. (f) Gütlich, P.; Hauser, A.; Spiering, H. *Angew. Chem., Int. Ed. Engl.* **1994**, *33*, 2024−2054. (g) Sato, O. *Acc. Chem. Res.* **2003**, *36*, 692−700. (h) Real, J. A.; Gaspar, A. B.; Niel, V.; Muñoz, M. C. *Coord. Chem. Rev.* **2003**, *236*, 121−141. (i) *Spin Crossover in Transition Metal Compounds I−III*; Gütlich, P., Goodwin, H. A., Eds.; Topics in Current Chemistry, Vols. *233−235*; Springer: Berlin, 2004. (j) Real, J. A.; Gaspar, A. B.; Muñoz, M. C. *Dalton Trans.* **2005**, 2062−2069. (k) Halcrow, M. A. *Polyhedron* **2007**, *26*, 3523−3576. (l) Nihei, M.; Shiga, T.; Maeda, Y.; Oshio, H. *Coord. Chem. Rev.* **2007**, *251*, 2606−2621. (m) Gamez, P.; Sánchez-Costa, J.; Quesada, M.; Aromí, G. *Dalton Trans.* **2009**, 7845−7853. (n) Halcrow, M. A. *Coord. Chem. Rev.* **2009**, *253*, 2493−2514. (o) Olguin, J.; Brooker, S. *Coord. Chem. Rev.* **2011**, *255*, 203−240. (p) Bousseksou, A.; Molnár, G.; Salmon, L.; Nicolazzi, W. *Chem. Soc. Rev.* **2011**, *40*, 3313−3335. (q) Muñoz, M. C.; Real, J. A. *Coord. Chem. Rev.* **2011**, *255*, 2068−2093. (r) *Spin Crossover Materials: Properties and Applications*; Halcrow, M. A., Ed.; Wiley: Chichester, U.K., 2013.

(2) (a) Cambi, L.; Szegö, L. *Ber. Dtsch. Chem. Ges.* **1931**, *64*, 2591−2598. (b) Cambi, L.; Szegö, L. *Ber. Dtsch. Chem. Ges.* **1933**, *66*, 656−661. (c) Cambi, L.; Malatesta, L. *Ber. Dtsch. Chem. Ges.* **1937**, *70*, 2067−2078.

(3) van Koningsbruggen, P. J.; Maeda, Y.; Oshio, H. *Top. Curr. Chem.* **2004**, *233*, 259−324.

(4) (a) Simaan, A. J.; Boillot, M. L.; Rivière, E.; Boussac, A.; Girerd, J. J. *Angew. Chem., Int. Ed.* **2000**, *39*, 196−198. (b) Simaan, A. J.; Boillot, M.-L.; Carrasco, R.; Cano, J.; Girerd, J.-J.; Mattioli, T. A.; Ensling, J.; Spiering, H.; Gütlich, P. *Chem.—Eur. J.* **2005**, *11*, 1779−1793. (c) Floquet, S.; Simaan, A. J.; Rivière, E.; Nierlich, M.; Thuéry, P.; Ensling, J.; Gütlich, P.; Girerd, J. J.; Boillot, M. L. *Dalton Trans* **2005**, 1734−1742.

(5) Ellison, M. K.; Nasri, H.; Xia, Y. M.; Marchon, J. C.; Schulz, C. E.; Debrunner, P. G.; Scheidt, W. R. *Inorg. Chem.* **1997**, *36*, 4804−4811.

(6) Goldsmith, C. R.; Jonas, R. T.; Stack, T. D. P. *J. Am. Chem. Soc.* **2002**, *124*, 83−96.

(7) Bautz, J.; Comba, P.; Que, L., Jr. *Inorg. Chem.* **2006**, *45*, 7077−7082.

(8) (a) Bernal, I.; Jensen, I. M.; Jensen, K. B.; McKenzie, C. J.; Toftlund, H.; Tuchagues, J. P. *J. Chem. Soc., Dalton Trans.* **1995**, 3667−3675. (b) Simaan, A. J.; Banse, F.; Girerd, J. J.; Wieghardt, K.; Bill, E. *Inorg. Chem.* **2001**, *40*, 6538−6540. (c) Nielsen, A.; Larsen, F. B.; Bond, A. D.; McKenzie, C. J. *Angew. Chem., Int. Ed.* **2006**, *45*, 1602−1606. (d) Nebe, T.; Beitat, A.; Würtele, C.; Dücker-Benfer, C.; Van Eldik, R.; McKenzie, C. J.; Schindler, S. *Dalton Trans.* **2010**, *39*, 7768−7773.

(9) Mialane, P.; Nivorojkine, A.; Pratviel, G.; Azéma, L.; Slany, M.; Godde, F.; Simaan, A.; Banse, F.; Kargar-Grisel, T.; Bouchoux, G.; Sainton, J.; Horner, O.; Guilhem, J.; Tchertanova, L.; Meunier, B.; Girerd, J. J. *Inorg. Chem.* **1999**, *38*, 1085−1092.

(10) Ortega-Villar, N.; Ugalde-Saldívar, V. M.; Muñoz, M. C.; Ortiz-Frade, L. A.; Alvarado-Rodríguez, J. G.; Real, J. A.; Moreno-Esparza, R. *Inorg. Chem.* **2007**, *46*, 7285−7293.

(11) Ortega-Villar, N.; Thompson, A. L.; Muñoz, M. C.; Ugalde-Saldívar, V. M.; Goeta, A. E.; Moreno-Esparza, R.; Real, J. A. *Chem.—Eur. J.* **2005**, *11*, 5721−5734.

(12) Ortega-Villar, N. A.; Muñoz, M. C.; Real, J. A. *Eur. J. Inorg. Chem.* **2010**, 5563−5567.

(13) Martin, J. P.; Zarembowitch, J.; Bousseksou, A.; Dworkin, A.; Haasnoot, J. G.; Varret, F. *Inorg. Chem.* **1994**, *33*, 6325−6333.

(14) Slichter, C. P.; Drickamer, H. G. *J. Chem. Phys.* **1972**, *56*, 2142−2143.

(15) Haddad, M. S.; Lynch, M. W.; Federer, W. D.; Hendrickson, D. N. *Inorg. Chem.* **1981**, *20*, 123−231.

(16) The EPR spectra were simulated using: *WIN-EPR SimFonia software*, version 1.2; Bruker Instruments, Inc.: Billerica, MA, 1995.

(17) (a) Oshio, H.; Toriumi, K.; Maeda, Y.; Takashima, Y. *Inorg. Chem.* **1991**, *30*, 4252−4260. (b) Conti, A. J.; Chadha, R. K.; Sena, K. M.; Rheingold, A. L.; Hendrickson, D. N. *Inorg. Chem.* **1993**, *32*, 2670−2680. (c) König, E. *Prog. Inorg. Chem.* **1987**, *35*, 527−622. (d) Dorbes, S.; Valade, L.; Real, J. A.; Faulmann, C. *Chem. Commun.* **2005**, 69−71. (e) Tanimura, K.; Kitashima, R.; Bréfuel, N.; Nakamura, M.; Matsumoto, N.; Shova, S.; Tuchagues, J. P. *Bull. Chem. Soc. Jpn.* **2005**, *78*, 1279−1282. (f) Nemec, I.; Herchel, R.; Boča, R.; Trávníček, Z.; Svoboda, I.; Fuess, H.; Linert, W. *Dalton Trans.* **2011**, *40*, 10090−10099. (g) Vieira, B. J. C.; Coutinho, J. T.; Santos, I. C.; Pereira, L. C. J.; Waerenborgh, J. C.; da Gama, V. *Inorg. Chem.* **2013**, *52*, 3845−3850.

(18) For example, see: (a) Shipilov, V. I.; Zelentsov, V. V.; Zhdanov, V. M.; Turdakin, V. A. *JETP Lett., Engl. Transl.* **1974**, *19*, 294−295. (b) Conti, A. J.; Kaji, K.; Nagano, Y.; Sena, K. M.; Yumoto, Y.; Chadha, R. K.; Rheingold, A. L.; Sorai, M.; Hendrickson, D. N. *Inorg. Chem.* **1993**, *32*, 2681−2693. (c) Sorai, M.; Maeda, Y.; Oshio, H. *J. Phys. Chem. Solids* **1990**, *51*, 941−951. (d) Floquet, S.; Boillot, M. L.; Rivière, E.; Varret, F.; Boukheddaden, K.; Morineauc, D.; Négrier, P. *New J. Chem.* **2003**, *27*, 341−348. (e) Tang, J.; Sánchez-Costa, J.; Smulders, S.; Molnár, G.; Bousseksou, A.; Teat, S. J.; Li, Y.; van Albada, G. A.; Gamez, P.; Reedijk, J. *Inorg. Chem.* **2009**, *48*, 2128−2135. (f) Yemeli, E. W. T.; Blake, G. R.; Douvalis, A. P.; Bakas, T.; Alberda van Ekenstein, G. O. R.; van Koningsbruggen, P. J. *Chem.—Eur. J.* **2010**, DOI: 10.1002/chem.201002100.

(19) Ugur, I.; Marion, A.; Parant, S.; Jensen, J. H.; Monard, G. *J. Chem. Inf. Model.* **2014**, *54*, 2200−2213.

(20) Cao, C.; Yuan, H.; Liu, S.; Zheng, R. *J. Chem. Inf. Comput. Sci.* **2000**, *40*, 1010−1014.

(21) Salmon, L.; Molnár, G.; Zitouni, D.; Quintero, C.; Bergaud, C.; Micheaud, J. C.; Bousseksou, A. *J. Mater. Chem.* **2010**, *20*, 5499−5503.

(22) Langford, C. H.; Chung, F. M. *J. Am. Chem. Soc.* **1968**, *90*, 4485−4486.

(23) *CrysAlis CCD and CrysAlis RED*; Oxford Diffraction Ltd: Abingdon, U.K., 2007.

(24) Clark, R. C.; Reid, J. S. *Acta Crystallogr.* **1995**, *A51*, 887−897.

(25) Sheldrick, G. M. *SHELXS97 and SHELXL97*; University of Göttingen: Göttingen, Germany, 2008.

(26) Farrugia, L. J. *J. Appl. Crystallogr.* **1997**, *30*, 565−566.

(27) Farrugia, L. J. *J. Appl. Crystallogr.* **1999**, *32*, 837−838.

(28) *CRC Handbook of Chemistry and Physics*, 90th ed.; Weast, R. C., Ed.; CRC Press: Boca Raton, FL, 2010.

DOI: 10.1021/ic503081x
Inorg. Chem. XXXX, XXX, XXX−XXX